A New Global Ionospheric Electron Density Model Based on Grid Modeling Method

Huijun Le[1,2,3,5], Tingwei Han[1,2,5], Libo Liu[1,2,3,5], Yiding Chen[1,2,4,5], Hui Zhang[1,2,3,5]

[1] Key Laboratory of Earth and Planetary Physics, Institute of Geology and Geophysics, Chinese Academy of Sciences, Beijing, 100029, China

[2] Institutions of Earth Science, Chinese Academy of Sciences

[3] Mohe National Geophysical Observatory, Institute of Geology and Geophysics, Chinese Academy of Sciences, Beijing, 100029, China

[4] Beijing National Observatory of Space Environment, Institute of Geology and Geophysics, Chinese Academy of Sciences, Beijing, 100029, China

[5] College of Earth and Planetary Sciences, University of the Chinese Academy of Sciences, Beijing 100049, China

Corresponding author: Huijun Le (lehj@mail.iggcas.ac.cn)

Key Points:

- A new global ionosphere empirical modeling method is proposed.
- Global modeling is decomposed into three-dimensional grid-point independent modeling
- The new model can effectively preserve the regional differences of ionosphere

Abstract:

Based on nearly 4.6 million radio occultation ionospheric profile data from COSMIC satellites in 2006-2020, a global three-dimensional ionospheric electron density model was constructed by a new concept. The global 3D ionosphere structure was divided into total 338,661 grids with longitude intervals of 10 degrees, latitude intervals of 2 degrees, and height intervals of 5 km. Each individual grid model is first constructed, and then all grid models are combined to form a global ionospheric model. Each grid model has 21 coefficient for modeling solar activity, geomagnetic activity, local time, and season variation.This method makes full use of all ionospheric electron density data without any spatial smoothing, and can effectively model the fine ionospheric spatial structure like longitudinal wavenumber-4 structure in low latitudes. The model also takes into account the influence of both solar and geomagnetic activities on the ionosphere. It can give the climatological variation of ionospheric electron density with geomagnetic activity. In addition, by combined with the International Reference Ionospheric electron density results of E layer below 140km, the problem of three-peak error of occultation data below peak height of F2 layer in middle and low latitude region is effectively solved, and accurate low-altitude profile data can be obtained. Compared with other data sources such as ZH01 and ROCSAT-1, the simulation ability of the model in fine spatial structure is verified.

1. Introduction

The Earth's ionosphere is full of charged particles, which can reflect and modify radio waves used for radio communication, navigation, and operation of the satellite navigation systems like GPS, GLONASS, BEIDOU, and GALILEO. The ionosphere is also the most closely region related to human activities in space. Many of our Earth-orbiting satellites hang out there, including the International Space Station and China Space Station. these satellites add spacecrafts can also be affected by the various changes in the ionosphere, including sudden swells of charged particles that increase drag on satellites and shorten their orbital lifetimes. Therefore, there is a growing demand for understanding and forecasting the ionosphere. The ionosphere is affected by solar radiation, solar wind, geomagnetic storms, as well as the energy propagating upward from lower atmosphere. The ability to model and eventually anticipate the solar cycle, annual, semi-annual and seasonal variations as well as irregularities in ionosphere is of great use for both ionospheric research and space weather applications. A variety of ground-based and space-based detection devices have been developed internationally, and many local and global ionospheric empirical models have been constructed based on these observations (e.g. Gowtam et al., 2019; Hoque and Jakowski, 2011; Li et al., 2021; Kutiev et al., 2009; Le et al., 2017; Themens et al., 2017).

Since the 1990s, GPS has been gradually applied to ionospheric observations.The time delay and phase shift obtained by the dual-frequency receiver can obtain a high accuracy of the total ionospheric electron content.With the increase of ground-based GPS receivers, these rich ionospheric observations have greatly improved our understanding and knowledge of the ionosphere.Many ionospheric empirical models are also constructed based on these GPS/TEC data. The GPS/TEC method also has some limitations. On the one hand, it can only get the total integrated electron content without the electron density height profile information. On the other hand, due to the limitations of topography, the receiver can only be placed on land, so a large number of data over the ocean are missing. The application of radio occultation technology in atmospheric and ionospheric detection can effectively

remedy the above two deficiencies. On the one hand, the information of ionospheric electron density height profile can be obtained by occultation method, although there are some errors in low altitude. On the other hand, occultation observations are not affected by topography and has good global coverage.

According to the characteristics of ionospheric observation data, there are many methods to construct regional or global empirical model of ionospheric electron density, including spherical harmonic function method, empirical orthogonal function, custom fitting function, etc. All of these methods perform a degree of fitting and smoothing of the observed data and may therefore lose some local features. If the globe is evenly divided into sufficiently fine grids, and there is enough data in each grid to create a separate model for each grid, then the grid models can be aggregated to form a global ionospheric model. This is a new concept of ionospheric empirical modeling. This new grid modeling method can make full use of all observation information and avoid using the same function to fit all latitude and longitude data. That is, this method can effectively preserve the regional differences of ionosphere. If we have enough data in global range, we can use this method to construct a high accuracy model. We name this method as Grid Modelling.

The Constellation Observing System for Meteorology, Ionosphere, and Climate (COSMIC) is a constellation of six small satellites that study Earth's atmosphere and ionosphere. These satellites were lunched in 2006 and then continue operate until now. The electron density profiles derived from the occultation observations have reached more than 4.6 million. These data are enough for us to carry out Grid Modeling.

2. Data Source

The COSMIC occultation data were used in this ionospheric empirical modeling work. The electron density height profiles can be calculated by Radio Occultation method. The COSMIC electron density data cover long time of more than one solar cycle from 2006 to 2019. The electron density height profiles of total 4.6 million were used in the modeling work. For each ionospheric electron density height profile, electron density at various heights from 140 km to 700 km with 5 km interval were interpolated. Thus the ionosphere is binned into 113 heights. At each fixed height,

there are about 4.6 million electron density data. Then we can get about 520 million data points. These data have good coverage in longitude, latitude, local time, season, solar activity, geomagnetic activity and so on. Figure 1 shows the distribution of the COSMIC electron density data in these respects.

Solar radiation flux at 10.7cm band was used to characterize solar activity. F107 is a daily solar activity index used as an input parameter in many ionospheric empirical and theoretical models (e.g., Hedin et al., 1996; Picone et al., 2002; Titheridge, 1997; Yue et al., 2008) to represent changes in solar activity. F107A is the 81-day moving average value of daily F107 index. F107P is the mean value of daily F107 and its 81-day moving average F107A. The F107P index has been verified to be a better solar EUV proxy for ionosphere modeling and ionospheric investigations (e.g. Liu et al., 2006, 2009; Ma et al., 2009; Ikubanni and Adeniyi, 2017). Thus, the F107P index is used here to model solar activity variation of ionospheric electron density. In addition, the Kp index is used here to model geomagnetic activity variations of ionospheric electron density.

To verify the model results, we also selected the radio occultation data of China Seismo-Electromagnetic Satellite/ZhangHeng-01 (CSES / ZH01) with a similar orbit height to COSMIC. The orbit locates at an altitude of about 507 km. The CSES satellite was launched on Feb 2, 2018. It has a Sun-synchronous orbit. Its descending/ascending node is at1400 LT/0200 LT. The CSES radio occultation data only cover the low solar activity period of 2018-2020. We also selected the total ion density data of ROCSAT-1 satellite to check the IGGM model results with non radio occultation data. ROCSAT-1 was launched on January 27, 1999. Its orbit height was 600 km and its orbit inclination was 35°. Thus it can only cover the low latitudes within ±35°. The ionospheric plasma and electrodynamics instrument (IPEI) onboard the satellite consists of four sensors to measure the ion concentration, the ion temperature, and the ion drift velocity vector. Here we used the data of total positive ion density which is basically equal to electron density according to the principle of electric neutrality of ionosphere charged particles.

3. Model Construction

The model constructed in this paper is based on the Grid Modeling approach, so the model is named Ionosphere Global Grid Model (IGGM). To simulate the global ionospheric electron density variation, we divide the globe into many grids according to longitude, latitude and height, and model each grid point separately. The global ionosphere is divided into 37 longitude planes (from -180 degrees to 180 degrees with 10 degrees interval), 81 latitude zones (from -80 degrees to 80 degrees with 2 degrees interval) and 113 heights in altitude (from 140 km to 700 km with 5 km interval).There are total of 338,661 grid points in the global ionosphere model. Figure 2 illustrates the grid distribution of the model.

The ionospheric electron density was modeled for each grid point. First of all, all electron density data near the grid point (The longitudinal range is ± 7.5 degrees and latitudinal range is ± 2 degrees) are selected as the observation data of the grid point. There are 4.6 million observations worldwide, with approximately 4,800 observations at each grid point. The model of each grid point can then be constructed based on the fitting method. Because we have decomposed global ionospheric modeling into sufficiently fine grid modeling, the modeling for each grid mainly simulates solar activity, geomagnetic activity, seasonal and local time variations. The model equation is as follows:

$$\begin{cases} Ne_{global} = \bigcup Ne_{ijk}, \quad Ne_{ijk} = A_{n1} \cdot A_{n2} \cdot A_{n3} \\ A_{n1} = c_{n11} + c_{n12} \cdot F107P + c_{n13} \cdot F107P^2 + c_{n14} \cdot Kp + c_{n15} \cdot Kp^2 \\ A_{n2} = 1 + \sum_{m=1}^{4} c_{n21m} \cdot \cos(\frac{2\pi \cdot m \cdot DOY}{365}) + c_{n22m} \cdot \sin(\frac{2\pi \cdot m \cdot DOY}{365}) \\ A_{n3} = 1 + \sum_{m=1}^{4} c_{n31m} \cdot \cos(\frac{2\pi \cdot m \cdot LT}{24}) + c_{n32m} \cdot \sin(\frac{2\pi \cdot m \cdot LT}{24}) \end{cases} \quad (1)$$

The Ne_{ijk} is the electron density model at a fixed grid of longitude *i*, latitude *j* and altitude *k* (*i=1, ... , 37; j=1, ... , 81; k=1, ... , 113*). The A_{n1}, A_{n2} and A_{n3} represent the solar cycle & geomagnetic variation, seasonal variation and local time variation, respectively (e.g., Xu and Kamide, 2004; Ercha et al., 2012; Le et al., 2017). For each grid model, we calculated values of the 21 coefficients in the formula above through solving nonlinear curve-fitting problems in least-squares sense. The global model

IGGM have total of 7,111,881 coefficients. Based on these coefficients, we can calculate the three-dimensional distribution of global ionospheric electron density for a given solar activity, geomagnetic activity, season, local time/universe time. Meanwhile, peak density NmF2, peak height hmF2 and total electron content (from 140 km to 700km) can also be calculated.

Abel Inversion of ionospheric electron density height profile by radio occultation requires some assumption (Schreiner et al., 1999; Let al., 2007; Straus, 2007; Yue et al., 2010), including spherical symmetric distribution of electron density, straight line signal propagation, and first order estimate of the electron density at the top. Spherical symmetry assumption is thought to be the major error source (Straus et al., 2007). In fact, ionospheric electron density is not symmetrically distributed, and the asymmetry is more pronounced at lower latitudes (et al. Straus, 2007; Yue et al., 2010). Therefore, the COSMIC electron density data has a large error below the peak height at low latitudes (e.g. Yue et al., 2011). It is well known that ionosphere electron density has a significant two-peak EIA structure at low latitudes, but the COSMIC data show a significant spurious three-peak structure (Yue et al., 2010). To solve this problem, we will use a combination of the International Reference Ionospheric (IRI) model results at the E-layer and IGGM data near the peak height. The low-altitude ionosphere of E layer is mainly controlled by photochemical process, and IRI-2012 model (Bilitza et al., 2014) can give more accurate results. The radio occultation data near and above the peak height are also more accurate. Therefore, IRI-2012 model results at heights of 100 km − 140 km will be used, IGGM model results above hmF2-30 will be used, and curve fitting method will be used to calculate the electron density between 140 km and hmF2-30. Therefore, the lower boundary of IGGM model is extended from 140km to 100km after combination with IRI model results.

4. Results and Model Validation

The electron density variations of IGGM model without combination with IRI-2012 results is plotted in Figure 3. For comparison, the electron density variations of IGGM model with combination with IRI-2012 results is also plotted in Figure 3. One can find significant error of three peaks at low heights of low latitudes in the

IGGM results without combination with IRI-2012 results. After combination with low-altitude data from the IRI2012 model, the IGGM results significantly corrected the spurious three-peak structure below the F2-layer peak height at low latitudes.

Figure 4 shows the IGGM modeled NmF2 results at night time (LT=0.0) in March equinox (Doy=82) under low solar activity (F107=80), middle solar activity (F107=130), and high solar activity (F107=180). The IGGM results show significant longitudinal structure of wavenumber-4 in low latitudes under all solar activity conditions from low solar activity to high solar activity. The longitudinal wavenumber-4 variation is more prominent in low solar activity. In addition, the IGGM model results show significant Weddell Sea Anomaly (40°-60° S latitude and 75°-120° W longitude) with electron density enhancements in nighttime. Many previous studies reported such a night enhancement at middle latitudes (e.g. Chang et al., 2015; Chen et al., 2016; He et al., 2009; Jee et al., 2009; Klimenko et al., 2015). Our model results also shows more remarkable enhancement in higher solar activity. The IGGM model results also illustrate the significant ionospheric middle trough structure with a minimum at geomagnetic latitude 50°-70° at nighttime. The peak latitudes have no solar activity dependence, which is consistent with previous studies (e.g. Le et al., 2016; Yang et al., 2015). Figure 5 illustrates the model results in daytime (LT=12) in March equinox (Doy=82) under low solar activity (F107=80), middle solar activity (F107=130), and high solar activity (F107=180). we also can find the significant longitudinal wavenumber-4 structure.

IGGM model is not only a model of geomagnetic quiet period, this model takes Kp as geomagnetic activity index and considers the influence of different geomagnetic activities. In order to test the effect of this model on geomagnetic activity simulation, we also established a model without considering geomagnetic activity. Figure 6 shows the relative error of NmF2 in high geomagnetic activity (Kp>3) of the IGGM results with considering Kp and without considering Kp. By comparing the model errors with and without the influence of geomagnetic activity, we find that the IGGM model can significantly reduce the model errors by considering the influence of Kp, especially the larger error rate. The average absolute

relative error decreases from 33% of the Kp effect not taken into account to 20% of the Kp effect included. The rate of percentage error of 95% decrease from 1.41% to 0.62%. Ionospheric disturbances or ionospheric storms have very complex temporal and spatial variations during geomagnetic activity. IGGM model can only give the average variation characteristics of geomagnetic disturbances. Nevertheless, the model can give the ionospheric disturbances in different regions roughly.

To further verify IGGM model results, we selected two types of observation results and an empirical model (IRI-2012) for comparative analysis. The two observations are ZH01 occultation observation and ROCSAT-1 in-situ observation. ZH01 satellite has a similar orbital altitude to COSMIC satellite. Therefore, ZH01 occultation observations should be close to COSMIC occultation results. ZH01 is a sun-synchronous satellite with only two local time intervals (1400 LT and 0200LT). This study mainly uses the 1400 LT results. Figure 7 shows the comparison between NmF2 calculated by IGGM model and ZH01 satellite observation results, as well as the comparison with IRI-2012 model results. It is clear from these comparisons that the NmF2 calculated by the IGGM model is very close to the ZH01 observations in terms of latitude variation and longitude structure. However, the results calculated by IR-2012 are quite different from those observed by ZH01 in both latitude variation and longitude structure. Table 1 shows the detailed comparison of error of NmF2 between IRI model results and ZH01 observations and between IGGM model results and ZH01 observations. The percentage error of IGGM model is ~ 10% at low latitudes and ~20% at middle latitudes. But that of IRI-2012 model is more than 40% at both low latitudes and middle latitudes.

Figure 8 shows the comparison between hmF2 calculated by IGGM model and ZH01 satellite observation results, as well as the comparison with IRI-2012 model results. The comparisons show that the hmF2 of IGGM model is very close to that of the ZH01 observation. But there are significant differences between the IRI model results and the ZH01 observation. The detailed differences of hmF2 are listed in Table 1. The hmF2 error of IGGM model is larger (~ 20 km) at low latitudes and smaller at (less than 15 km) at middle latitudes. The hmF2 error of IRI model has no latitude

dependence. It is larger than 30 km at all latitudes. The results as illustrated in Figures 7 and 8 suggest that the IGGM model can well reproduce the major features of ionospheric F2 layer observed by ZH01, but IRI model does not reproduce the observation well.

The IGGM model covers an altitude range of 100-700 km. ROCSAT-1's orbit height is about 600 km. Thus, ROCSAT-1 observations of electron density in the top ionosphere were selected to further check the IGGM model's ability to simulate the top ionosphere. First, we compared the global distribution of ROCSAT-1 electron density in different seasons with that of IGGM model and IRI model. The comparisons are shown in Figure 9. The results of IGGM model and ROCSAT-1 have almost the same longitude variation, but the latitude structure of low latitude is slightly different. ROCSAT-1 observations show that the electron density at 600km still has two peak structures at some longitude sectors, but the IGGM model shows a single peak structure. The IRI model also shows a single peak structure. Figure 10 shows the comparison of local time and latitudinal variation of ROCSAT-1 electron density with that of IGGM model and IRI model. It is clear that the IGGM model's latitudinal variation and local time is more close to the observations of ROCSAT-1 than IRI model's result.

A major difference is that the electron density values in the IGGM model are lower than those observed in ROCSAT-1. The electron density value of IRI mode is also lower than the ROCSAT-1 observation, but the same as that of IGGM model. There are two possible reasons for this difference. On the one hand, ROCSAT-1 observation period was from 1999 to 2004, while COSMIC data used for IGGM modeling covered 2006-2019. That is to say, the two data sets are in two different solar activity cycles, and the ionospheric variations in the two solar activity cycles are different. On the other hand, ROCSAT-1 is the total ion density observed in situ, while COSMIC result is the electron density profile of radio occultation inversion. The difference in observation principle and instrument error leads to the difference in electron density. Nevertheless, Figures 9 and 10 show consistent seasonal differences in IGGM model, ROCSAT-1 observation, and IRI model, with the highest electron

density in March equinox and September equinox, and the lowest electron density in June solstice.

One advantage of using Grid Modelling method to develop global or regional ionospheric models like IGGM model is that there is not much fitting or smoothing in spatial structure. This kind of model preserves more spatial structural features. Based on the same COSMIC radio occultation data, we also established a global ionospheric model by using empirical orthogonal function (EOF) method (Li et al., 2021). Figure 11 shows a comparison of the simulation results of the two models. We can see that the longitude structure of IGGM model NmF2 and hmF2 is relatively fine, and the ionospheric wavenumber-4 structure can be clearly seen in NmF2 and hmF2. However, the EOF model does not show a similar structure and the result is more smooth.

Finally, we compared the calculated results of the IGGM model with COSMIC data used to build the model, and verify the model's ability to reproduce the observed data. Figure 12 shows histogram distribution of percentage error between IGGM model and all the COSMIC observation data in low geomagnetic activity (Kp<3). We can find the IGGM model can reproduce the observations used in the model very well. The correlation coefficient between model NmF2 and observed NmF2 is more than 0.93. The mean of percentage error of NmF2 between model and observation is about 15%. The mean of error of hmF2 is about 11 km. The detailed error distribution of NmF2, hmF2, and Ne at heights from 300 km to 700 km is listed in Table 2. The results in Table 2 show that the percentage error decreases with height. About 40-50% of the error value of NmF2 and Ne at fixed height is within 15%. And about 90% of the error value of NmF2 and Ne at fixed height is within 55%. As for hmF2, almost all of the errors are less than 55km, and 70% of the errors are within 15km. In addition, we calculate the daytime (08LT - 16LT) and nighttime (20LT - 04LT) error distributions respectively. Figure 13 illustrates the comparison of of error distribution of NmF2 and hmF2 between IGGM model and COSMIC observation in daytime and in nighttime. The results show that both of the NmF2 error and hmF2 error are significantly lower in daytime than in nighttime. The average error of NmF2 was

about 13.9% in the daytime and 20.6% in the nighttime. The average error of hmF2 was about 10.5km in the daytime and 14.3km in the nighttime. On the one hand, this may be due to the lower electron density at night, so the percentage error is larger; on the other hand, the nighttime ionospheric behaviors are more complicated and the variations are larger.

5. Summary

Ionospheric empirical models are very useful and important platforms and tools for ionospheric climatology and ionospheric space weather applications. Based on various kinds of ionosphere data and methods, the researchers have constructed many regional and global ionospheric empirical models. The COSMIC occultation satellites have accumulated a large amount of ionosphere electron density profile data over a decade of continuous running. Based on these large number of data, we have proposed a new method (Grid Modelling) for modeling the global ionospheric temporal and spatial variations.The core idea of Grid Modeling is to decompose global ionospheric modeling into single grid-point modeling in sufficiently fine grid points. In this way, the spatial structure information can be retained to the maximum extent. In this study, the global ionosphere model was divided into 338,661 grid points with interval of 10 degrees in longitude, 2 degrees in latitude and 5 km in height. Each local grid point model was constructed to model season, local time, solar activity, and geomagnetic variations of ionospheric electron density in each grid point. Then all grid point models are combined to form the IGGM model. The advantage of this modeling is that it only needed to be fitted in temporal variations, not needed to be fitted in spatial variations. Thus it can get more accurate spatial structures of ionosphere.

Due to the inherent defects of the algorithm for retrieving ionospheric electron density profile from radio occultation observations, false three-peak structure is prone to appear in the ionospheric data at low latitude.Through data fusion processing with the results of the international reference ionospheric IRI-2012 model, we solved the problem of the forged three-peak structure. At the same time, we further verified the high accuracy of the model in simulating ionospheric spatial structure by comparing it

with different data, such as ZH01 and ROCSAT-1 satellite data. Finally, the error analysis between the model results and the observation data used for modeling shows that the error of NmF2 of all data is less than 20%, and the error of daytime is less than 15%, and the error of peak height is less than 13km. IGGM model can output ionospheric climatologic changes quickly and effectively, and it also has many applications in space weather. For example, we are taking IGGM model results as the background field of ionospheric data assimilation, and GPS TEC and occultation TEC data as the observation field to study ionospheric daily variations.

Acknowledgement:

We acknowledge COSMIC team for providing the electron density profile data (https://cdaac-www.cosmic.ucar.edu/cdaac/). The CSES/ZH01 radio occultation data can be downloaded from the official website (www.leos.ac.cn). The ROCSAT-1 data can be downloaded from the website (https://cdaweb.gsfc.nasa.gov/pub/data/formosat-rocsat/formosat-1/). This research was supported by the National Key Research and Development Program (2018YFC1503504), B-type Strategic Priority Program of the Chinese Academy of Sciences (XDB41000000), National Natural Science Foundation of China (41822403, 41774165), and Youth Innovation Promotion Association CAS.

References

A, E., D. Zhang, A. J. Ridley, Z. Xiao, and Y. Hao (2012), A global model: Empirical orthogonal function analysis of total electron content 1999–2009 data, J. Geophys. Res., 117, A03328, doi:10.1029/2011JA017238.

Bilitza, D., D. Altadill, Y. Zhang, C. Mertens, V. Truhlik, P. Richards, L.-A. McKinnell, and B. Reinisch (2014), The International Reference Ionosphere 2012 - a model of international collaboration, J. Space Weather Space Clim., 4, A07, 1-12, doi:10.1051/swsc/2014004.

Chang, L. C., H. Liu, Y. Miyoshi, C.-H. Chen, F.-Y. Chang, C.-H. Lin, J.-Y. Liu, and Y.-Y. Sun (2015), Structure and origins of the Weddell SeaAnomaly from tidal and planetary wave signatures in FORMOSAT-3/COSMIC observations and GAIA GCM simulations, J. Geophys. Res.Space Physics, 120, 1325–1340, doi:10.1002/2014JA020752.

Chen, Y., L. Liu, H. Le, W. Wan, and H. Zhang (2016), The global distribution of the dusk-to-nighttime enhancement of summer NmF2at solarminimum, J. Geophys. Res. Space Physics, 121, 7914–7922, doi:10.1002/2016JA022670.

Gowtam, V. S., Tulasi Ram, S., Reinisch, B., & Prajapati, A. (2019). A new artificial neural network-based global three-dimensional ion-ospheric model (ANNIM-3D) using long-term ionospheric observations: preliminary results. Journal of Geophysical Research: Space Physics, 124(6), 4639 – 4657.

He, M., L. Liu, W. Wan, B. Ning, B. Zhao, J. Wen, X. Yue, and H. Le (2009), A study of the Weddell Sea Anomaly observed by FORMOSAT-3/COSMIC, J. Geophys. Res., 114, A12309, doi:10.1029/2009JA014175.

Hedin, A. E., E. L. Fleming, and A. H. Manson (1996), Empirical wind model for the upper, middle and lower atmosphere, J. Atmos. Terr. Phys.,58, 1421 – 1447.

Hoque, M. M., & Jakowski, N. (2011). A new global empirical NmF2 model for operational use in radio systems. Radio Science, 46, 1–13. doi:10.1029/2011rs004807.

Jee, G., A. G. Burns, Y.-H. Kim, and W. Wang (2009), Seasonal and solar activity variations of the Weddell Sea Anomaly observed in the TOPEXtotal electron

content measurements, J. Geophys. Res., 114, A04307, doi:10.1029/2008JA013801.

Klimenko, M. V., V. V. Klimenko, and A. T. Karpachev (2015), Spatial features of Weddell Sea and Yakutsk Anomalies in foF2diurnal variationsduring high solar activity periods: Interkosmos-19 satellite and ground-based ionosonde observations, IRI reproduction and GSM TIPmodel simulation, Adv. Space Res., 55, 2020–2032, doi:10.1016/j.asr.2014.12.032.

Kutiev, I., Marinov, P., Belehaki, A., Reinisch, B., & Jakowski, N. (2009). Reconstruction of topside density profile by using the topside sounder model profiler and digisonde data. Advances in Space Research, 43(11), 1683–1687, doi:10.1016/j.asr.2008.08.017

Le, H., L. Liu, X. Yue, and W. Wan (2008), The ionospheric responses to the 11 August 1999 solar eclipse: Observations and modeling, Ann. Geophys., 26, 107–116.

Le, H., N. Yang, L. Liu, Y. Chen, and H. Zhang (2017), The latitudinal structure of nighttime ionospheric TEC and its empirical orthogonal functions model over North American sector, J. Geophys. Res. Space Physics, 122, 963–977, doi:10.1002/2016JA023361.

Lei, J., et al. (2007), Comparison of COSMIC ionospheric measurements with ground-based observations and model predictions: Preliminary results, J. Geophys. Res., 112, A07308, doi:10.1029/2006JA012240.

Li, Q., Liu, L., He, M., Huang, H., Zhong, J., Yang, N., Zhang, M., Jiang, J., Chen, Y., Le, H., Cui, J. (2021). A global empirical model of electron density profile in the F region ionosphere basing on COSMIC measurements. Space Weather, 19, e2020SW002642, doi:10.1029/2006JA012240.

Liu, L., W. Wan, B. Ning, O. M. Pirog, and V. I. Kurkin (2006), Solar activity variations of the ionospheric peak electron density, J. Geophys. Res., 111, A08304, doi:10.1029/2006JA011598.

Liu, L., and Y. Chen (2009), Statistical analysis of solar activity variations of total electron content derived at JetPropulsion Laboratory from GPS observations, J.

417 Geophys. Res., 114, A10311, doi:10.1029/2009JA014533.
418 Ma, R., J. Xu, W. Wang, and W. Yuan (2009), Seasonal and latitudinal differences of
419 the saturation effect between ionospheric NmF2and solar activity indices, J.
420 Geophys. Res., 114, A10303, doi:10.1029/2009JA014353.
421 Picone, J. M., A. E. Hedin, D. P. Drob, and A. C. Aikin (2002), NRLMSISE-00
422 empirical model of the atmosphere: Statistical comparisons and scientific issues,
423 J. Geophys. Res., 107(A12), 1468, doi:10.1029/2002JA009430.
424 Schreiner, W. S., S. V. Sokolovskiy, C. Rocken, and D. C. Hunt (1999), Analysis and
425 validation of GPS/MET radio occultation data in the ionosphere, Radio Sci.,
426 34(4), 949–966, doi:10.1029/1999RS900034.
427 Straus, P. R. (2007), Ionospheric climatology derived from GPS occultation
428 observations made by the ionospheric occultation experiment, Adv. Space Res.,
429 39, 793–802, doi:10.1016/j.asr.2006.08.009.
430 Themens, D. R., Jayachandran, P. T., Galkin, I., & Hall, C. (2017). The empirical
431 Canadian high Arctic ionospheric model (E-CHAIM): NmF2 and hmF2. Journal
432 of Geophysical Research: Space Physics, 122, 9015–9031,
433 doi:10.1002/2017JA024398.
434 Titheridge, J. E. (1997), Model results for the ionospheric E-region: Solar and
435 seasonal changes, Ann. Geophys., 15, 63 – 78.
436 Xu, W., and Y.Kamide (2004), Decomposition of daily geomagnetic variations by
437 using method of natural orthogonal component, J. Geophys. Res., 109, A05218,
438 doi:10.1029/2003JA010216.
439 Yue, X., W. Wan, L. Liu, H. Le, Y. Chen, and T. Yu (2008), Development of a middle
440 and low latitude theoretical ionospheric model and an observation system data
441 assimilation experiment, Chin. Sci. Bull., 53(1), 94–101.
442 Yue, X., W. S. Schreiner, J. Lei, S. V. Sokolovskiy, C. Rocken, D. C. Hunt, and Y.-H.
443 Kuo (2010), Error analysis of Abel retrieved electron density profiles from radio
444 occultation measurements, Ann. Geophys., 28, 217–222,
445 doi:10.5194/angeo-28-217-2010.
446 Yue, X., W. S. Schreiner, Y.-C. Lin, C. Rocken, Y.-H. Kuo, and B. Zhao (2011), Data

447 assimilation retrieval of electron density profiles from radio occultation
448 measurements, J. Geophys. Res., 116, A03317, doi:10.1029/2010JA015980.
449 Ikubanni, S.O. and Adeniyi, J. O. (2017), Relationship between ionospheric F2-layer
450 critical frequency, F10.7, and F10.7P around African EIA trough, Adv. Space.
451 Res. 59(4), 1014-1022
452

453 **Table 1.** Comparison of Error of NmF2 and hmF2 between IRI model results and
454 ZH01 observations and between IGGM model results and ZH01 observations.
455

Latitude (°)	Error of NmF2 (%)		Error of hmF2 (km)	
	Error between IRI and ZH01	Error between IGGM and ZH01	Error between IRI and ZH01	Error between IGGM and ZH01
[40 60]	172.1	33.1	52.9	7.1
[20 40]	64.4	12.9	34.4	12.5
[0 20]	47.3	11.8	41.1	21.4
[-20 0]	48.8	10.5	37.3	23.6
[-40 -20]	59.1	22.7	32.1	14.1
[-60 -40]	98.9	25.6	41.1	9.8

456
457

458 **Table 2**. The error distribution of hmF2, NmF2, and Ne at fixed heights of 300km,
459 400km, 500km, 600km, and 700km.

	mean of absolute error (% or km)	Occurence of error within 15% or 15km	Occurence of error within 25% or 25km	Occurence of error within 35% or 35km	Occurence of error within 45% or 45km	Occurence of error within 55% or 55km
hmF2	11.2	66.1	85.1	93.2	96.7	98.3
NmF2	15.9	47.4	69.5	82.9	89.8	93.3
Ne (300km)	19.2	40.3	61.2	75.3	83.8	88.6
Ne (400km)	18.9	41.1	61.8	75.8	84.4	89.2
Ne (500km)	18.3	42.1	63.2	77.1	85.4	90.1
Ne (600km)	17.7	43.4	64.6	78.4	86.4	91.2
Ne (700km)	17.1	44.1	65.3	79.2	87.2	92.1

460

461

Figures

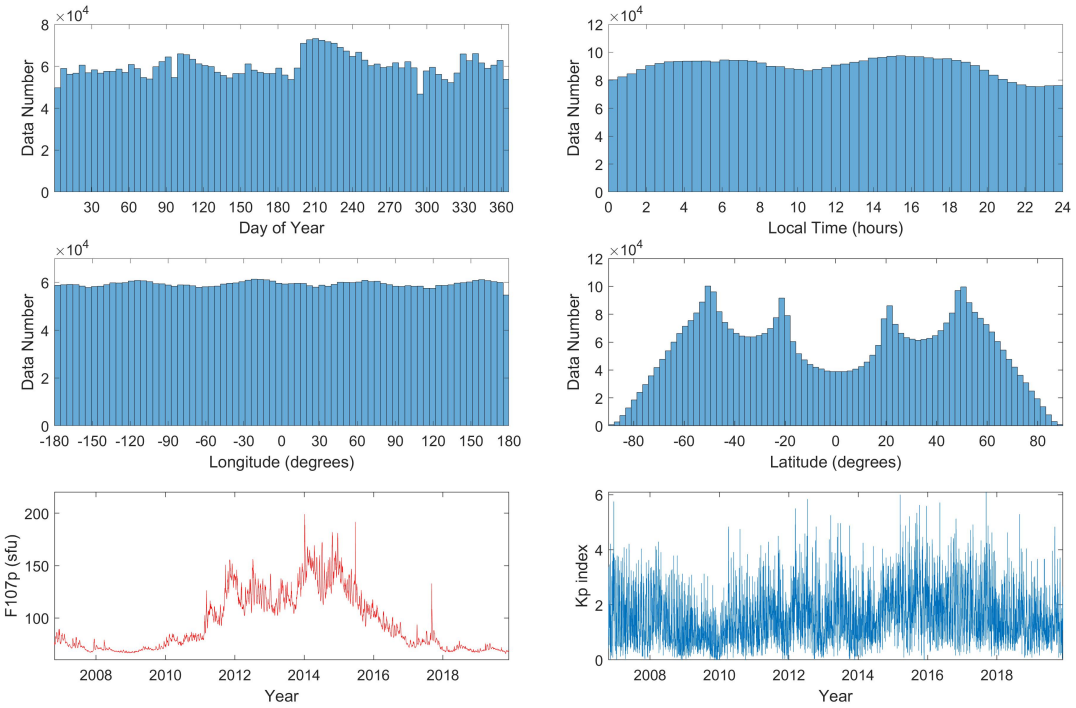

Figure 1. COSMIC radio occultation data distribution with season, local time, longitude and latitude. Temporal variations of solar activity index F107 and geomagnetic activity index Kp from 2006 to 2019.

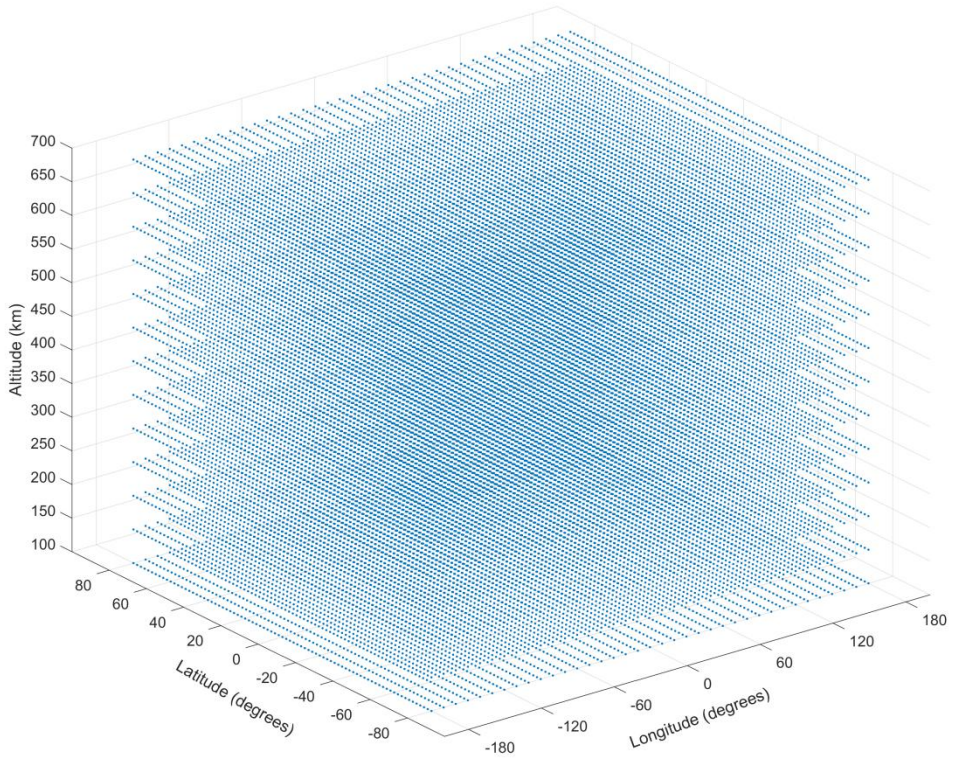

Figure 2. Grid point diagram of IGGM model.

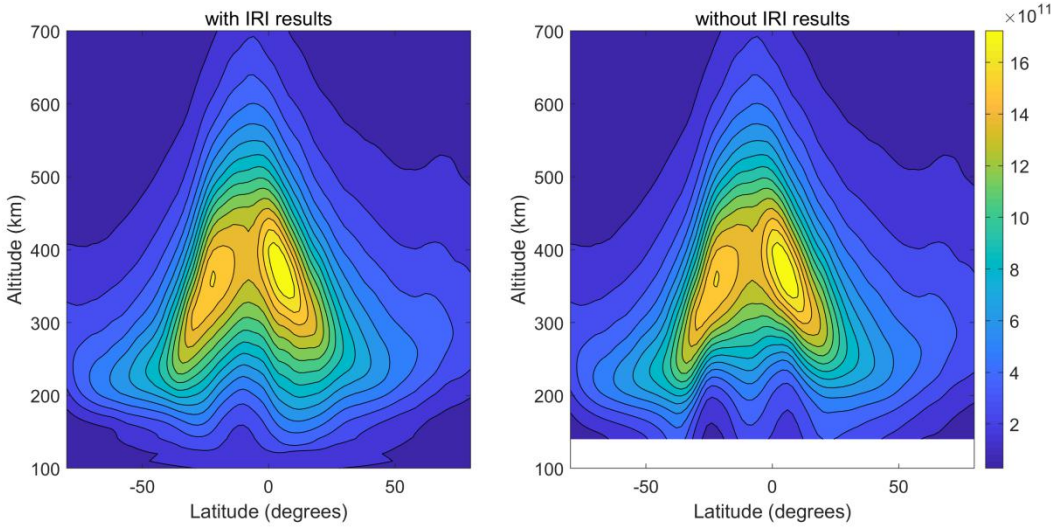

Figure 3. Comparison of ionospheric electron density height profiles between combination with IRI model results (left panel) and no combination with IRI model results (right panel). The figure shows the results of longitude -90°, 1400 LT, march equinox (DOY=82), solar activity F107=120, and geomagnetic activity Kp=0.

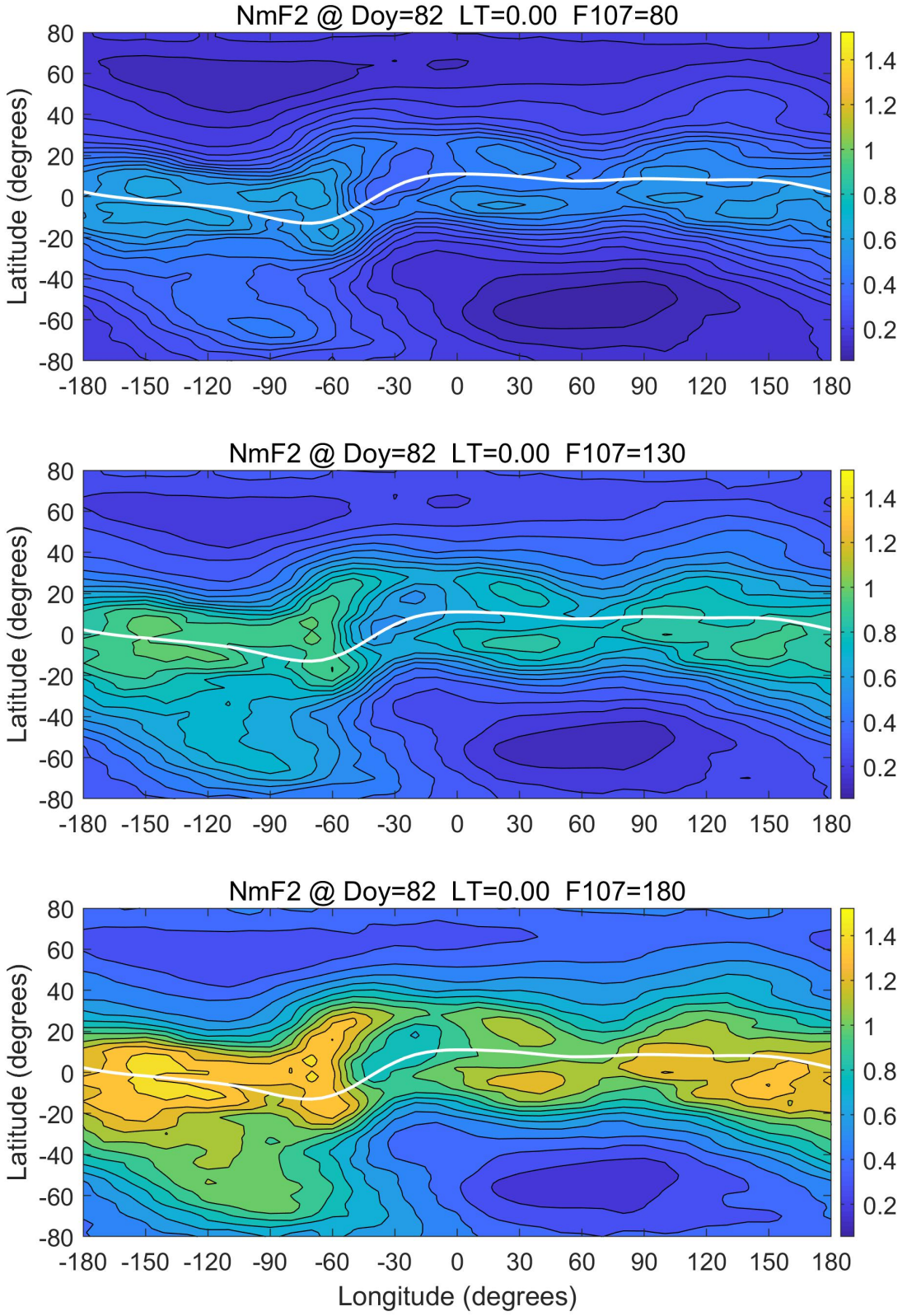

476

477 **Figure 4.** The spatial distribution of IGGM model NmF2 results at LT=0.0 in March
478 equinox Doy=82 under low solar activity (F107=80), middle solar activity
479 (F107=130), and high solar activity (F107=180). The unit is 1×10^{12} el/m^3.

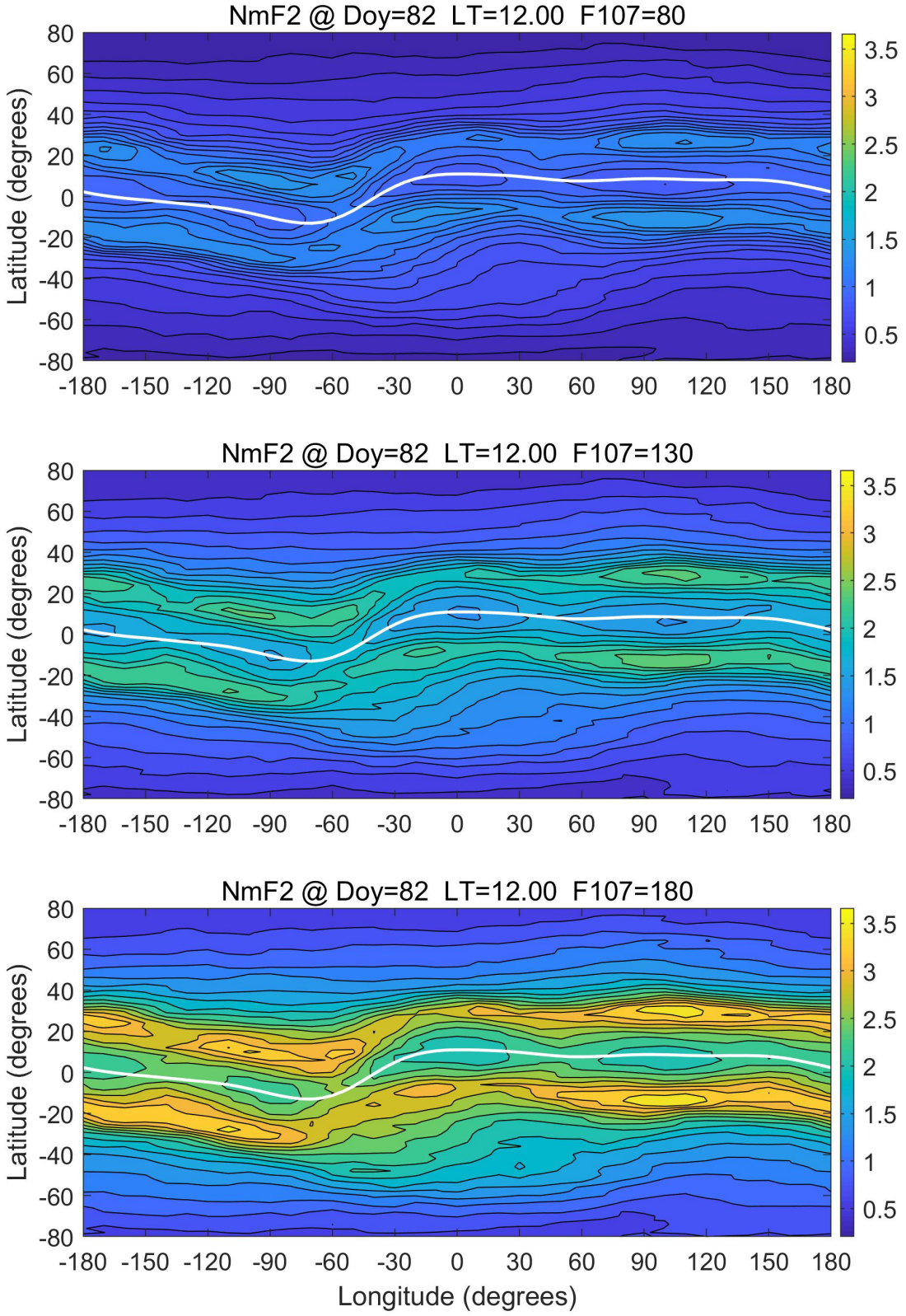

480
481 **Figure 5.** Same as Figure 4, but for daytime LT=12.0
482

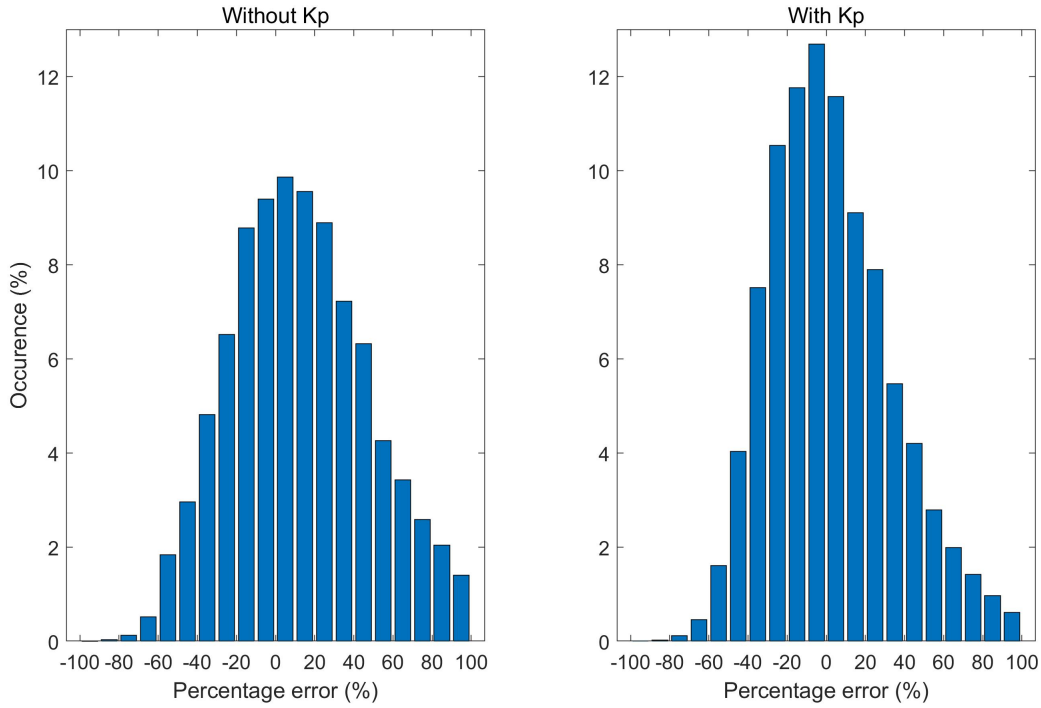

Figure 6. The relative error of NmF2 in high geomagnetic activity (Kp>3) between IGGM model results and COSMIC radio occultation observation. Left panel: the model results without considering Kp's influence. Right panel: the model results with Kp's influence

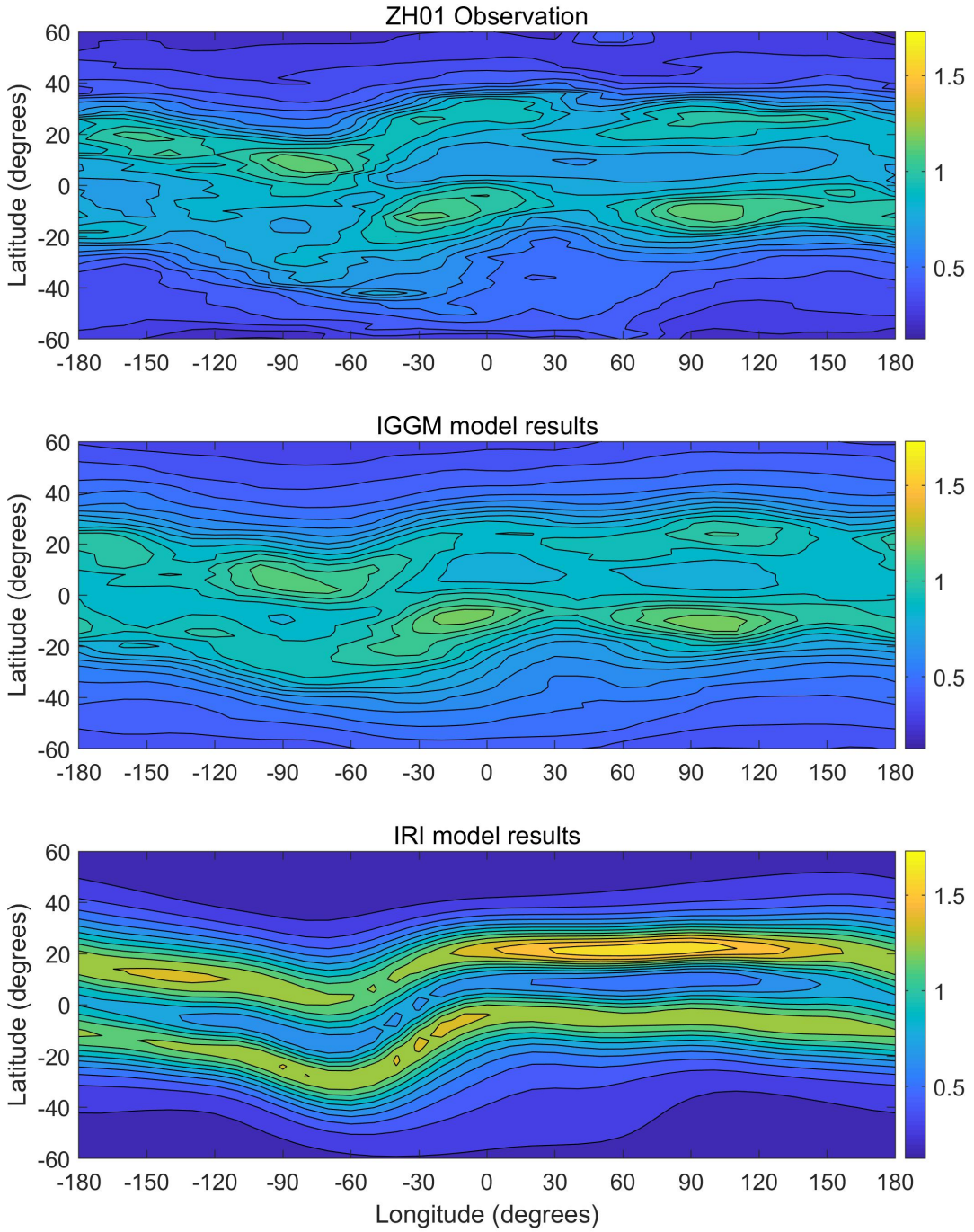

Figure 7. Comparison of NmF2 of IGGM model results with that of ZH01 observations and IRI model results. The ZH01 results are the 60-day average around March equinox (DOY 82±30). The modeled local time is 1400 LT, day of year is DOY=82, solar activity is F107=80. The unit of electron density is 10^{12} el/m^3.

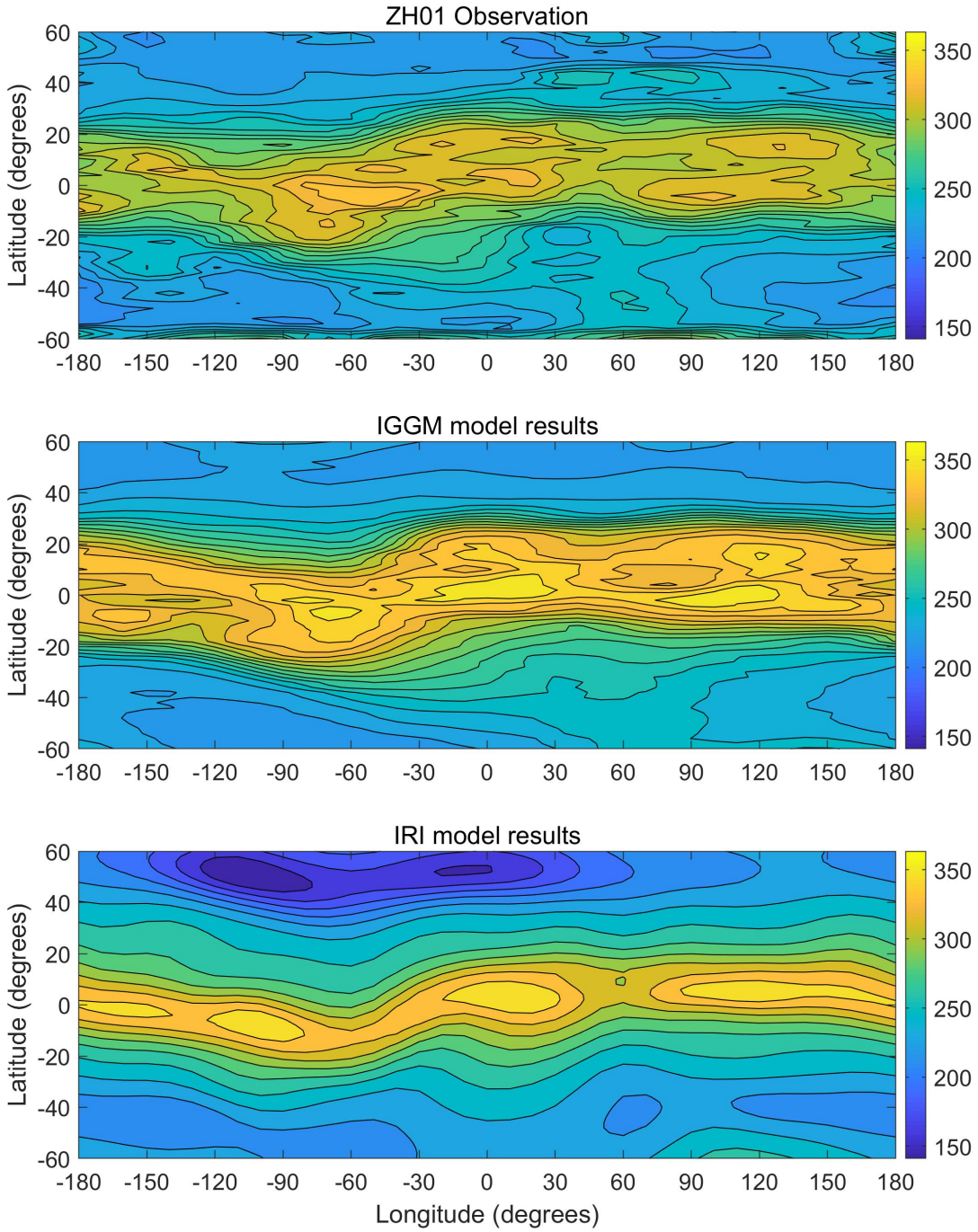

494

495 **Figure 8.** Same as Figure 7, but for hmF2.

496

497

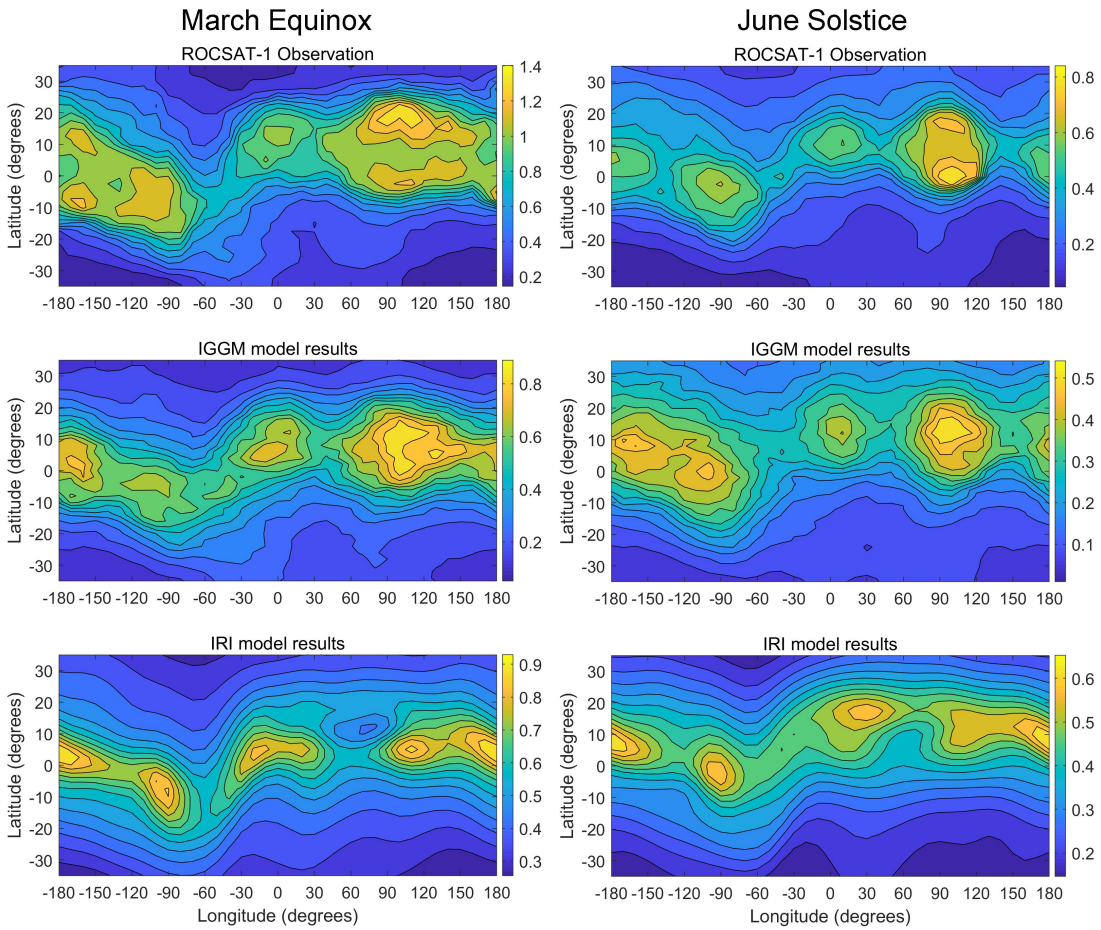

498

499 **Figure 9.** Comparison of topside electron density map of IGGM model with that of
500 ROCSAT-1 observations and with that of IRI model in March equinox and June
501 solstice. The ROCSAT-1 results are the 60-day average around March equinox (DOY
502 82±30) and around June equinox (DOY 173±30). The modeled local time is 1200 LT,
503 height is 600 km, and solar activity is F107=140. The unit of electron density is 10^{12}
504 el/m3.

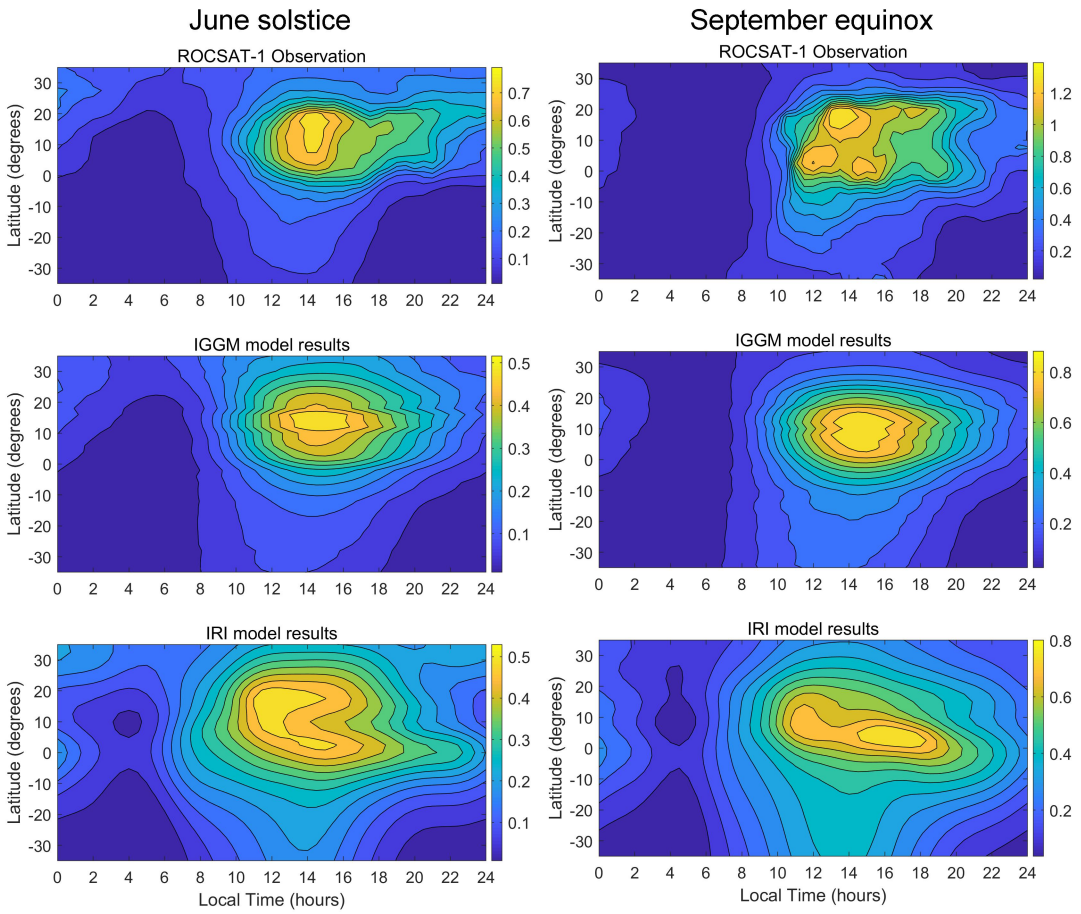

505

506 **Figure 10.** Comparison of topside electron density daily variation of IGGM model
507 with that of ROCSAT-1 observations and with that of IRI model in June solstice and
508 September equinox. The ROCSAT-1 results are the 60-day average around March
509 equinox (DOY 173±30) and around June equinox (DOY 263±30). The modeled local
510 time is 1200 LT, height is 600 km, and solar activity is F107=140. The unit of electron
511 density is 10^{12} el/m3.

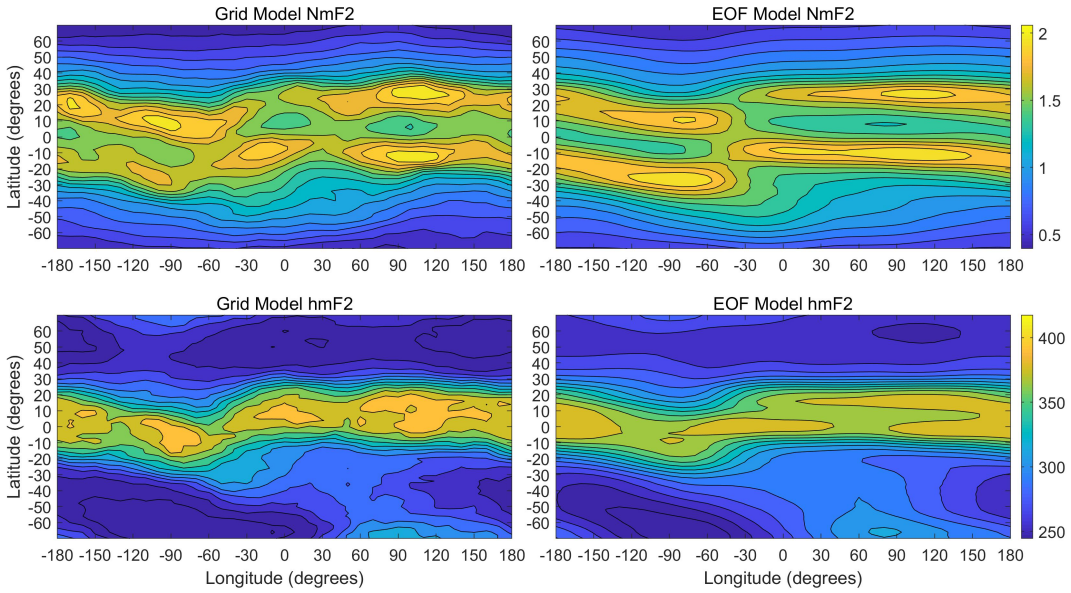

512

513 **Figure 11.** Comparison of model result of Grid model method with that of EOF
514 model method. Left panes show Grid model results. Right panels show EOF model
515 results. The unit of NmF2 is 10^{12}el/m^3. The unit of hmF2 is km. The simulation
516 condition: DOY=82, F107=120, and LT=12.

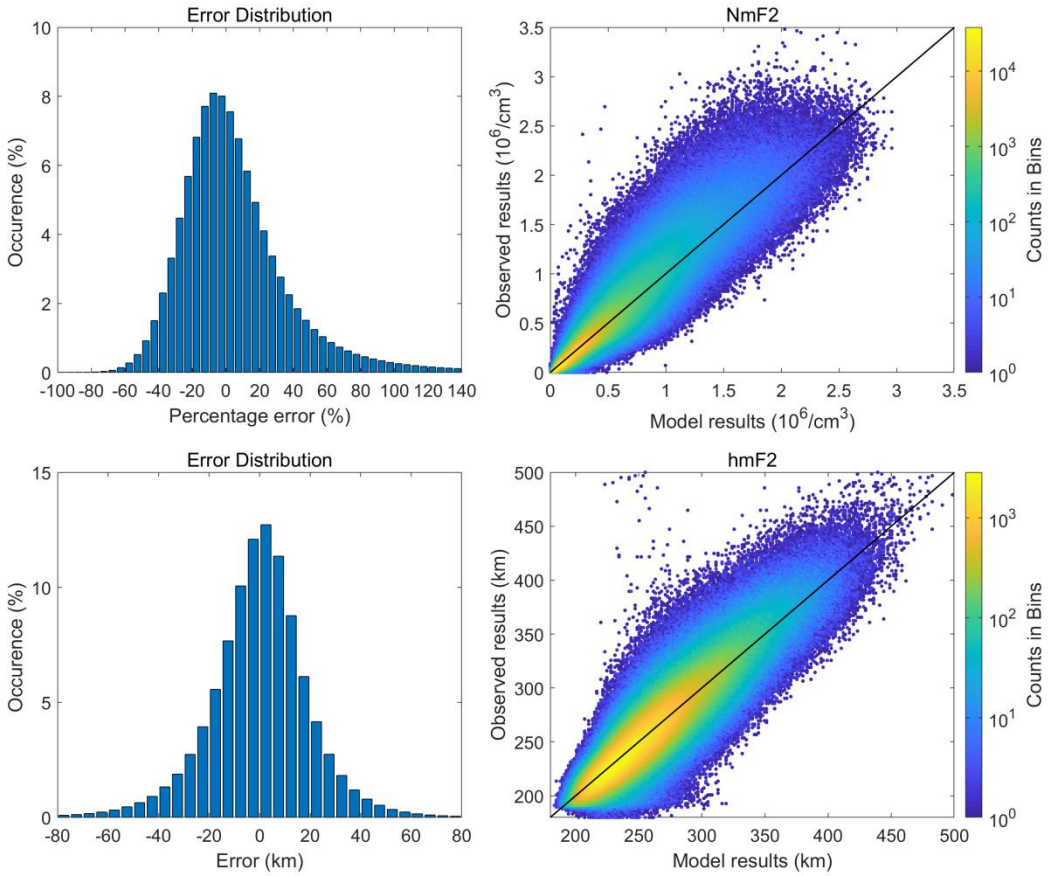

Figure 12. Comparison of NmF2 and hmF2 from IGGM model with that from COSMIC observations in low geomagnetic activity of Kp<3. (Left panels) The histogram distribution of percentage error between IGGM model and COSMIC observation. (Right panels) Bivariate histogram of comparisons between IGGM model and observations. The solid line shows the linear fitting of model and observation.

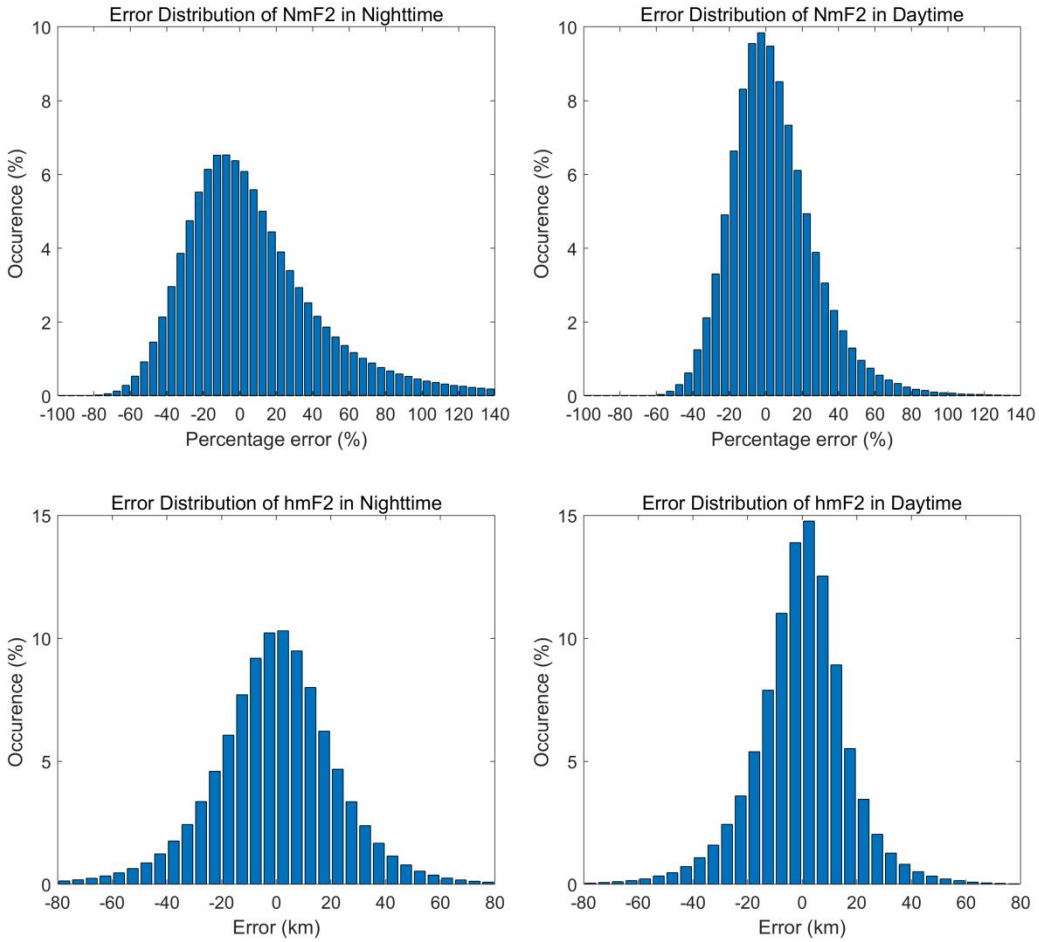

Figure 13. The comparison of error distribution of NmF2 and hmF2 between IGGM model and COSMIC observation in daytime (left panel) and in nighttime (right panel).